



ELSEVIER

Available online at www.sciencedirect.com

C. R. Mecanique 336 (2008) 224–231

<http://france.elsevier.com/direct/CRAS2B/>

Duality, inverse problems and nonlinear problems in solid mechanics

Initiation of geometric roughening in polycrystalline metal films

Guillaume Parry^a, Anthony G. Evans^b, John W. Hutchinson^{c,*}^a SIMAP/LTPCM, CNRS UMR 5266-INPG-UJF, 1130, rue de la Piscine, 38402 St Martin d'Hères, France^b Department of Materials, University of California, Santa Barbara, CA 93106, USA^c School of Engineering and Applied Sciences, Harvard University, Cambridge, MA 02138, USA

Available online 10 January 2008

Abstract

The mechanics of plasticity-induced roughening of initially planar polycrystalline metal films upon thermal cycling is presented. The emphasis is on films of FCC metals having grain size comparable to their thickness. In the model, the elastic substrate imposes a biaxial in-plane mismatch strain on the film. Calculations demonstrate how surface undulations develop with a length scale governed by the grain size, when plastic slip initiates above a critical strain. Under monotonic straining, the undulation amplitude grows in proportion to the imposed strain with extent dependent on the slip anisotropy. Upon cyclic plastic straining, three growth stages have been identified with the possibility of substantial roughness development. *To cite this article: G. Parry et al., C. R. Mecanique 336 (2008).*

© 2007 Académie des sciences. Published by Elsevier Masson SAS. All rights reserved.

Résumé

Initiation d'une rugosité en surface des films métalliques polycristallins. Un modèle décrivant l'apparition de rugosités de surface induites par mécanisme plastique pour des films métalliques polycristallins soumis à des cycles thermiques est présenté. Le modèle porte sur des métaux à structure CFC, avec une taille de grain de l'ordre de l'épaisseur du film. Le substrat impose une déformation biaxiale au film. Les calculs montrent que des ondulations se développent en surface lorsque le glissement plastique s'initie, au delà d'une déformation critique. Sous chargement monotone, l'amplitude des ondulations, dépendante de l'anisotropie plastique, augmente proportionnellement à la valeur de la déformation imposée. Sous chargement cyclique, trois stades de croissance de l'amplitude provoquant une rugosité marquée sont identifiés. *Pour citer cet article : G. Parry et al., C. R. Mecanique 336 (2008).*

© 2007 Académie des sciences. Published by Elsevier Masson SAS. All rights reserved.

Keywords: Solids; Thin films; Polycrystals; Plasticity; Surface roughness

Mots-clés : Solides ; Films minces ; Polycristaux ; Plasticité ; Rugosité de surface

1. Introduction

Polycrystalline metal films are used in a broad range of applications. Examples include: (i) Ni(Al) alloys used for oxidation protection of superalloy components in aero-engines [1], (ii) Cu and Al interconnects used in semiconductor devices [2,3]. In each case, the surface is susceptible to geometric roughening. That is, undulations develop having

* Corresponding author.

E-mail address: hutchinson@husm.harvard.edu (J.W. Hutchinson).

Nomenclature

F	Deformation gradient tensor	D	Symmetric part of the velocity gradient tensor
σ	Cauchy stress tensor	I	Second-order identity tensor
$\tau^{(\alpha)}$	Resolved shear stress on slip system α	C	Fourth-order elastic modulus tensor
$\mathbf{s}^{(\alpha)}$	Slip direction in slip system α	x_1, x_2, x_3	Cartesian coordinates
$\mathbf{m}^{(\alpha)}$	Normal to slip plane in slip system α	u_1, u_2, u_3	Displacement components expressed in Cartesian coordinates system
$\dot{\gamma}^{(\alpha)}$	Slip rate on slip system α		
ρ_0, ρ	Mass density in the reference and current state, respectively		

The tensor product of two vectors u and v is denoted $u \otimes v$. The inner product of two tensors S and T is denoted $S : T$.

amplitudes that increase during the life of the component, with adverse consequences for performance and durability. These geometric changes occur in accordance with three basic categories:

- *Category I: Isothermal roughening.* The misfit stress between the film and substrate, when sufficiently large, causes the strain energy contribution to the chemical potential to exceed the surface energy term. In such cases, at suitably elevated temperature, surface diffusion causes initial long wavelength undulations to increase their amplitude [4].
- *Category II: Cyclic ratcheting.* Upon thermal cycling, a strain misfit causes initial undulations to grow by a plasticity mechanism. This phenomenon is prevalent in aero-turbine systems, which use multilayers deposited on superalloy airfoils to provide thermal and oxidation protection. A model that characterizes this mechanism has been developed [5,6]. It provides both qualitative insights into the phenomenon, and quantitative predictions of the roles of the numerous parameters affecting the ratcheting rate. The model is limited to homogeneous layers, and requires initial geometric imperfections.
- *Category III: Plastic anisotropy.* In a polycrystalline layer, because of the differing orientations of slip systems in adjoining grains, grain-scale undulations develop on the surface [7]. This is the only category that enables undulations to emerge from initially planar surfaces.

The present assessment examines a category III mechanism by developing and implementing a three-dimensional finite-element, crystal-plasticity model that incorporates the effects of strain misfit and thermal cycling. Results are generated for a ‘representative FCC metal’, such as Al, Ni or Cu. The expectation is that these results will unearth general principles that can, thereafter, be applied to a broader range of systems.

This article is organized in the following manner. In Section 2, the model is described and the numerical procedure presented. Application of the model to a single thermal excursion is presented in Section 3 to duplicate isothermal undulation development. In Section 4, the response to strain cycling is examined, highlighting shakedown and ratcheting.

2. Polycrystalline model and numerical procedure

The constitutive framework comprises a rate-dependent crystallographic slip theory. The model is developed in a continuum context, without recognition of discrete dislocations. The resolved shear stress on each slip system provides the driving force for plasticity. A finite strain continuum formulation is employed which identifies the crystal lattice that can undergo elastic deformations and rotation [8]. Material flows through the crystal lattice by dislocation motion. The reference configuration is the undeformed crystal lattice. The current configuration is specified by the deformation gradient \mathbf{F} . An intermediate configuration is imagined, where the material flows through the undeformed lattice: \mathbf{F}^P denotes the plastic deformation gradient (shear) in this configuration. The current configuration is reached from this state by stretching and rotating the lattice, as well as the material contained in the lattice, with deformation gradient \mathbf{F}^* . The total deformation gradient is $\mathbf{F} = \mathbf{F}^* \mathbf{F}^P$.

The rate of \mathbf{F}^P is given by:

$$\dot{\mathbf{F}}^P(\mathbf{F}^P)^{-1} = \sum_{\alpha} \dot{\gamma}^{(\alpha)} \mathbf{s}^{(\alpha)} \otimes \mathbf{m}^{(\alpha)} \quad (1)$$

where $\mathbf{s}^{(\alpha)}$ and $\mathbf{m}^{(\alpha)}$ are expressed in the reference configuration. The relationship between stress and elastic strain increments is the generalized Hooke's law given by:

$$\hat{\sigma}^* + \sigma(\mathbf{I} : \mathbf{D}^*) = \mathbf{C} : \mathbf{D}^* \quad (2)$$

where, \mathbf{D}^* is the symmetric rate of stretching of the lattice, and $\hat{\sigma}^*$ is the co-rotational stress rate in the axis rotating with the lattice. The resolved shear stress on system (α) is given by:

$$\tau^{(\alpha)} = \frac{\rho_0}{\rho} \mathbf{m}^{*(\alpha)} \sigma \mathbf{s}^{*(\alpha)} \quad (3)$$

The superscript * on $\mathbf{s}^{(\alpha)}$ and $\mathbf{m}^{(\alpha)}$ indicates that those vectors are taken in the deformed configuration. Finally, the slip law is given by:

$$\dot{\gamma}^{(\alpha)} = \dot{\gamma}_0 \left| \frac{\tau^{(\alpha)}}{\tau_0} \right|^{(n-1)} \frac{\tau^{(\alpha)}}{\tau_0} \quad (4)$$

with $\dot{\gamma}_0$ and τ_0 as the reference strain-rate and flow stress, taken to be the same for all systems in this study. Recall that power law creep coincides with perfect plasticity when the exponent n is large. To clarify the basic mechanics, the present study excludes time dependence by employing large n : whereupon, effectively for each system

$$\dot{\gamma}^{(\alpha)} \geq 0, \quad \tau^{(\alpha)} = \tau_0; \quad \dot{\gamma}^{(\alpha)} \leq 0, \quad \tau^{(\alpha)} = -\tau_0; \quad \dot{\gamma}^{(\alpha)} = 0, \quad |\tau^{(\alpha)}| < \tau_0 \quad (5)$$

Creep effects can be readily incorporated in a subsequent assessment. Also for straightforwardness, the reference strain rate and the stress are taken to be temperature independent.

The basic model representing the polycrystalline film is depicted on Fig. 1. The grain size, L , is equated to the film thickness, h . This choice represents the microstructure commonly found when films experience elevated temperature during fabrication. The role of the substrate is to impose on the film an equi-biaxial mismatch strain, ε_m . For modeling simplicity, square grains are considered (Fig. 1) with two alternating orientations (A and B in Fig. 2). The grains are

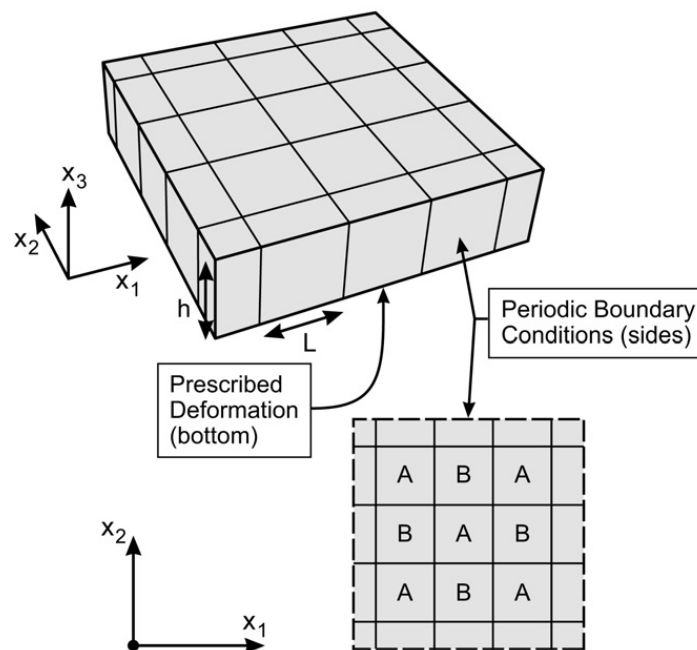


Fig. 1. Model for the bond coat. Calculations are made on a unit cell composed of two types of square grains with different orientations (A and B). Each grain extends through the film thickness (direction x_3). Displacements consistent with biaxial straining are applied on the bottom face to simulate the mismatch strains. Periodic boundary conditions are applied to the vertical faces.

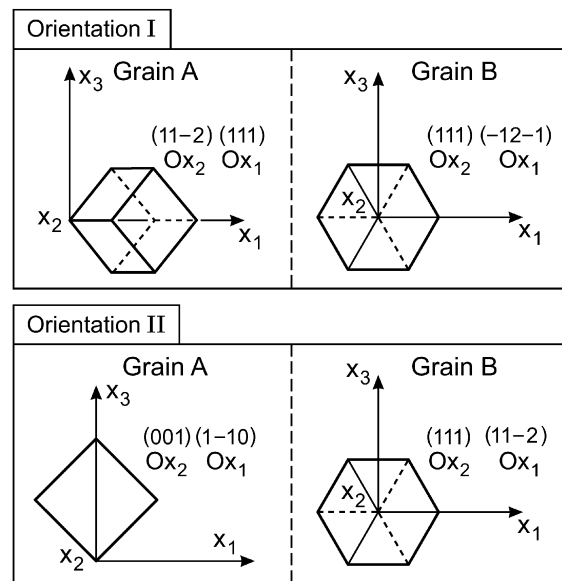


Fig. 2. Two orientation patterns for grains A and B are used within the calculations ('pattern I' and 'pattern II'). Film thickness is along the x_3 direction. Local (crystal) directions and corresponding global (x_1, x_2, x_3) directions are given, as well as representations of the cubic crystal coordinates with respect to the global system.

characterized by twelve slip systems of the $\{111\}\langle 011 \rangle$ family of an FCC crystal. Their elastic properties are isotropic and fully defined by the Young's modulus E and Poisson ratio ν .

Spatially periodic solutions exist, with characteristic length $2L$ (in x_1 and x_2). The periodicity relates to the chess-board distribution of the grains, as well as the uniform loading in the (x_1, x_2) plane. The periodic boundary conditions are visualized in Fig. 1 by means of a unit cell having double width, $w = 4L$. Traction along the upper and right faces equal those at corresponding points along the lower and left faces, respectively. The displacements, u_2 and u_3 , along the right face equal their counterparts along the left face at corresponding points: while u_1 on the right face equals u_1 on the left plus $\varepsilon_m w$. Displacements on the lower and upper faces are similarly related. At the bottom of the cell, where the crystals are bonded to the substrate, $u_3 = 0$. The in-plane displacements are prescribed in a manner consistent with the uniform biaxial strain ε_m .

The calculations are carried out by the finite element method using the ABAQUS software [9]. Finite displacements and strains are taken into account in the calculations. The single crystal constitutive law is implemented through a user subroutine [10]. For most computations, each grain was subdivided into 216 cubic elements. Two types of loading are considered:

- (i) *Monotonic*: the increase in mismatch strain corresponds to a film subjected a single thermal excursion.
- (ii) *Cyclic*: the strain is cycled repeatedly between 0 and ε_m , representative of the thermal cycling encountered in aero-engines.

The structure of the polycrystal is characterized by two orientations A and B: with the choice designated the "orientation pattern" (OP). Many patterns have been explored, giving similar trends. The two selected for presentation are referred to as orientations OP-I and OP-II (Fig. 2). Among the two, OP-II has the smaller plastic heterogeneity and less undulation development. Computations of the associated plastic slips and surface displacements reported below take $\tau_0/E = 0.08\%$ (representative of pure FCC metals, such as Al, Ni and Cu [11]).

3. Monotonic undulation growth

Initially, the system is stress free. A compressive biaxial misfit strain is imposed on the film and monotonically increased to $\varepsilon_m = 1\%$ (analogous to a single temperature excursion). As ε_m is increased, a periodic array of hillocks and depressions emerges on the surface with spacing set by the grain size (Fig. 3). An undulation amplitude, δ , is

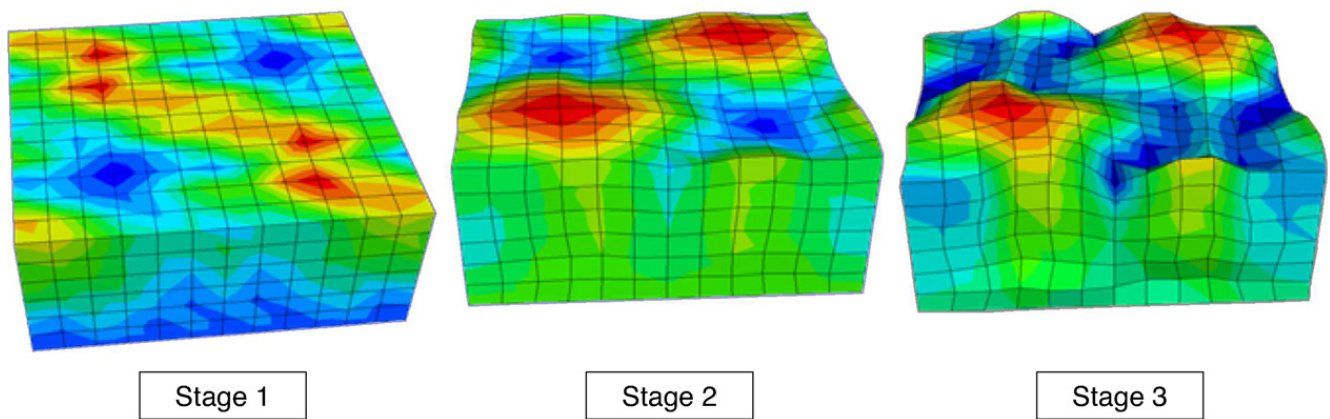


Fig. 3. Contour plots of the displacement normal to the surface. The shape of the surface during the three stages of amplitude evolution during cycling are reported for $\varepsilon_m = 1\%$ (orientation II, $\tau_0/E = 0.08\%$). Highest and lowest normal displacement areas are associated with red and blue respectively.

ascertained from the results, defined as the difference between the maximum vertical displacement at the top of the hillock and the minimum at the lowest point of the depression:

$$\delta = (u_3)_{\max} - (u_3)_{\min} \quad (6)$$

The evolution of the normalized undulation amplitude, δ/L , as ε_m is increased is plotted in Fig. 4(a) for the two orientation patterns. For $\varepsilon_m \leq \varepsilon_0 \cong 2\tau_0/E$ the system is elastic, and the surface remains planar. Thus, ε_0 becomes a measure of the mismatch strain associated with the onset of slip under monotonic loading. Thereafter, the amplitude increases linearly with ε_m . For OP-I, $\delta/L \rightarrow 2\%$ when $\varepsilon_m = 1\%$ (Fig. 4(a)). For perfect plasticity, linearity would be expected:

$$\frac{\delta}{L} \approx K \left(\varepsilon_m - \lambda \frac{\tau_0}{E} \right) \quad (7)$$

with K and λ being constants that depend on details of the grain orientations. The linear scaling of δ/L with ε_m emphasizes the geometric nature of the undulation growth, modulated by the degree of mis-orientation among neighboring grains. The dependence on τ_0/E for $\varepsilon_m = 1\%$ is plotted in Fig. 4(b).

4. Effect of cyclic straining

The substrate is submitted to compressive cyclic straining with mismatch varying between 0 and ε_m . The ensuing trends are depicted on Figs. 5 and 6. Their interpretation is informed by classic cyclic phenomena such as shakedown, cyclic plasticity and ratcheting. At small misfit strains, $\varepsilon_m < \varepsilon_{SD}$ (where $\varepsilon_{SD} \cong 2\varepsilon_0$), shakedown occurs (Fig. 5(a)). Namely, while plastic slip during the first cycle induces a small undulation, the subsequent response is elastic and, thereafter, the surface profile remains invariant.

Larger strains induce cycle-by-cycle plastic slip and undulation growth. The undulations develop in accordance with three stages (Fig. 6).

- *Stage I behavior* is displayed in Fig. 5(b). Starting from an undulation that forms on the first cycle, the undulation amplitude *decreases* slightly for a few cycles.
- *Stage II* commences after 5–10 cycles. It is characterized by steady-state growth per cycle. The associated ratcheting is illustrated in Fig. 5(c) where the history is shown of the undulation amplitude during cycles 38 to 40. Small elastic contributions to the undulation change occur because the surface is no longer planar. These coincide with segments of the cycle where $d(\delta/L)_{II}/d\varepsilon_m$ is small. Within the remaining segments, forward or reverse slip occurs on the active slip systems during each cycle, accompanied by positive and negative changes in the undulation amplitude. The consequence is a net increase in δ/L with each cycle. Over many cycles, growth rates representative of those in Fig. 5(c) can lead to large undulations, evident in Fig. 6. During this stage, the undulations remain relatively smooth (Fig. 3). Notably, the growth per cycle scales as: $d(\delta/L)_{II}/dN \sim \varepsilon_m$.

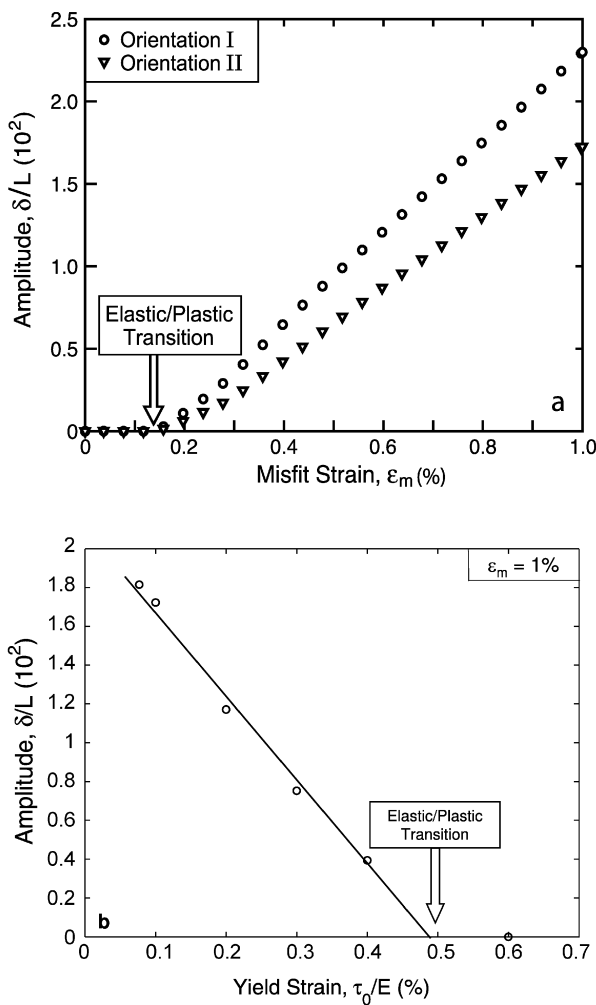


Fig. 4. Monotonic loading: (a) Evolution of the normalized undulation amplitude δ/L with respect to the mismatch strain ϵ_m (with $\tau_0/E = 0.08\%$) for orientation patterns I and II. Below the yield strain, the surface remains flat. Thereafter, δ/L increases linearly with ϵ_m (for $\epsilon_m = 1\%$, the undulations are $\sim 2\%$ of the grain size). (b) Undulation amplitude, normalized by yield strain, with $\epsilon_m = 1\%$ (orientation II).

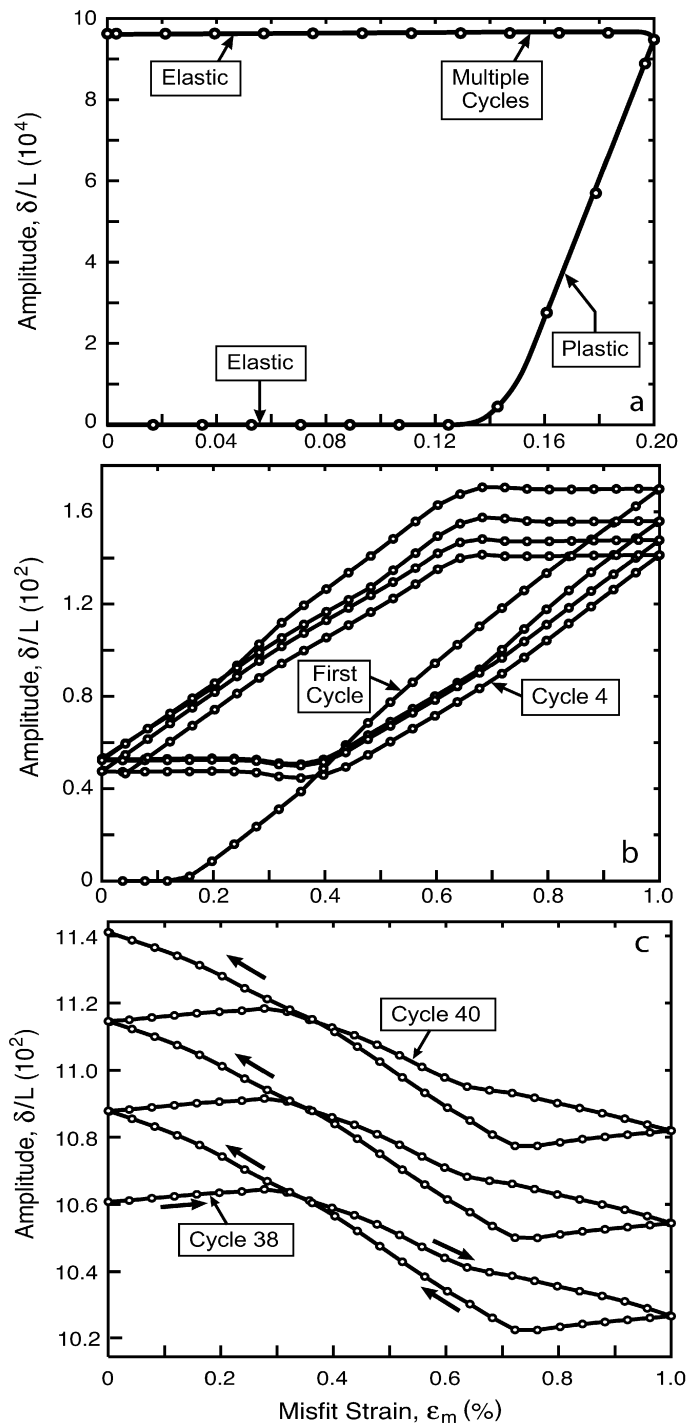


Fig. 5. Normalized undulation amplitude, δ/L , evolution with respect to the mismatch strain during cyclic loading (orientation II), $\tau_0/E = 0.08\%$. (a) Straining amplitude, $\epsilon_m = 0.2\%$. Shakedown behavior is observed resulting in elastic response after the first cycle. (b) Straining amplitude $\epsilon_m = 1\%$: The first four cycles display a slight decrease in amplitude after the first cycle. (c) Straining amplitude $\epsilon_m = 1\%$: ratcheting is observed, with undulations growth occurring on a cycle-by-cycle basis.

- *Stage III* is associated with the largest amplitudes, $\delta/L \geq 0.15$. At such amplitudes, the undulations develop steep surface slopes (Fig. 3). Finite geometry aspects and large rotations become important. The surface develops secondary roughness within individual grains, possibly the consequence of a surface instability. Even the locations

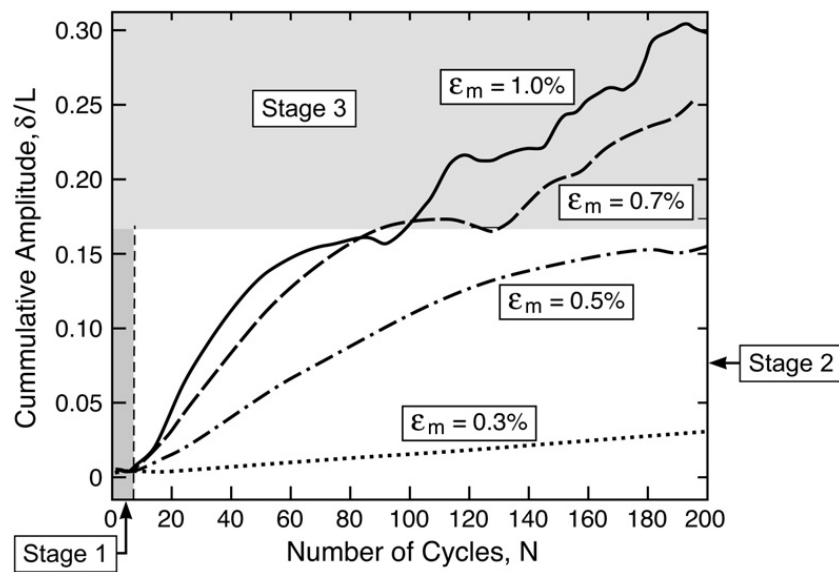


Fig. 6. Normalized undulation amplitude, δ/L , evolution with respect to the number of cycles N (orientation II, $\tau_0/E = 0.08\%$) for five strain amplitudes, ε_m . Three stages are identified. Unsteady undulation growth occurs during stage 1. Amplitude growth occurs on a cycle-by-cycle basis in stage 2. Growth is erratic in stage 3.

on the surface corresponding to the hillock maximum and the valley minimum used to define δ translate with cycling. These large-scale geometry changes are the source of the erratic growth found in this stage (Fig. 6). Schemes for further characterization of the undulation patterns are not apparent to the authors.

5. Concluding comments

The mechanics governing the development of undulations on the surface of an initially planar metal film has been presented. A model has been pursued for films having grain size of order the film thickness and implemented for elastic-perfectly plastic FCC metals. The calculations demonstrate how surface undulations develop due to slip anisotropy from grain to grain. Undulation growth commences when plastic slip initiates, above a critical biaxial mismatch strain, ε_m . For a single cycle, the undulation amplitude grows in proportion to ε_m with extent dependent on the slip anisotropy. Cycle-by-cycle undulation growth occurs whenever the mismatch strain exceeds the shakedown limit. Three stages have been identified. Stage I is a short transient involving deformation adjustments following plastic slip during the first cycle. Stage II involves steady-state ratcheting, with growth per cycle that scales with the misfit strain. When the amplitudes become large, stage III commences. In this stage large-scale geometry changes result in erratic shape evolutions that defy straightforward characterization.

Further work is required to fill out trends and quantitative details. Nevertheless, the present study provides convincing evidence that roughness of polycrystalline films develops from an initially planar surface due to single-crystal slip anisotropy, with wavelength that scales with the grain size. The implications of the present analysis for grain-dependent surface roughening can be most clearly found in the experimental measurements of Nucci et al. [3] conducted on Al lines. Contrary to comments made by these authors, the current analysis reveals that there is *sufficient slip anisotropy* in FCC systems to enable substantial surface shape evolution to take place on a grain-by-grain length scale. Examinations of the roles of Poisson ratio and elastic anisotropy are beyond the scope of the present article. These effects will be explored in a subsequent assessment. Note that, in the frame of the present hypotheses, the results should be most applicable to Al. The implication for thermal barrier systems that experience thousands of thermal cycles is that a natural source of non-planarity arises early in the lifetime, even if the system is initially planarized [5,12].

References

- [1] A.G. Evans, D.R. Mumm, J.W. Hutchinson, G.H. Meier, F.S. Pettit, Mechanisms controlling the durability of thermal barrier coatings, *Prog. Mater. Sci.* 46 (2001) 505–553.

- [2] A.S. Budiman, W.D. Nix, N. Tamura, B.C. Valek, K. Gadre, J. Maiz, R. Spolenak, J.R. Patel, Crystal plasticity in Cu damascene interconnect lines undergoing electromigration as revealed by synchrotron X-ray microdiffraction, *Appl. Phys. Lett.* 88 (2006) 233515.
- [3] J. Nucci, S. Krämer, E. Artz, Local strains measured in Al lines during thermal cycling and electromigration using convergent-beam electron diffraction, *J. Mater. Res.* 20 (7) (2005) 1851–1859.
- [4] R. Panat, K.J. Hsia, D.G. Cahill, Evolution of surface waviness in thin films via volume and surface diffusion, *J. Appl. Phys.* 97 (2005) 013521.
- [5] D.S. Balint, J.W. Hutchinson, An analytical model of rumpling in thermal barrier coatings, *J. Mech. Phys. Solids* 53 (2005) 949–973.
- [6] D.S. Balint, T. Xu, J.W. Hutchinson, A.G. Evans, Influence of bond coat thickness on cyclic rumpling of thermally grown oxides, *Acta Mater.* 54 (2006) 1815–1820.
- [7] Z. Zhao, R. Radovitzky, A. Cuitiño, A study of surface roughening in fcc metals using direct numerical simulation, *Acta Mater.* 52 (2004) 5791–5804.
- [8] J.R. Rice, Inelastic constitutive relations for solids: an internal-variable theory and its application to metal plasticity, *J. Mech. Phys. Solids* 19 (1971) 433–455.
- [9] ABAQUS software, version 6.6, Hibbit, Karlsson & Sorensen, Inc., 2006.
- [10] Y. Huang, A user-material subroutine incorporating single crystal plasticity in the ABAQUS finite element program, report for the Division of Applied Sciences, Harvard, 1991.
- [11] M.F. Ashby, *Materials Selection in Mechanical Design*, third ed., Butterworth–Heinemann, Oxford, 2005.
- [12] I.T. Spitsberg, D.R. Mumm, A.G. Evans, On the failure mechanisms of thermal barrier coatings with diffusion aluminide bond coatings, *Mater. Sci. Engrg. A* 394 (2005) 176–191.